PCCP

PAPER

View Article Online
View Journal | View Issue

Cite this: *Phys. Chem. Chem. Phys.*, 2020, **22**, 10526

Exciton transfer free energy from Car–Parrinello molecular dynamics†

Christian Schwermann and Nikos L. Doltsinis *

Received 27th November 2019,
Accepted 14th January 2020

DOI: 10.1039/c9cp06419b

rsc.li/pccp

A computational approach is presented which allows the calculation of free energies profiles for exciton transfer processes within the framework of *ab initio* molecular dynamics (AIMD) simulations, sampling both the electronic and the nuclear degrees of freedom. To achieve this, restraining potentials are imposed on the centres of maximally localized Wannier orbitals. The resulting quantum-mechanical orbital forces are derived analytically and implemented in an AIMD program. In analogy to classical umbrella sampling techniques, these restraints are used to control an exciton transfer by incrementally moving the Wannier centres corresponding to the electron–hole pair along a suitable reaction coordinate. The new method is applied to study exciton transfer between two stacked penta(3-methylthiophene) molecules as a function of intermolecular distance. From the resulting free energy profiles, exciton transfer rates and diffusion constants are estimated, which prove to be in line with experimental results.

1 Introduction

Excitons, *i.e.* bound electron–hole pairs, and their dynamics play a fundamental role in many areas of physics, (bio)chemistry and nanotechnology. In biology, for instance, light-driven processes are often triggered by the transfer of an exciton from an antenna protein to a chemical reaction centre (*e.g.* photosynthesis in green plants and phototropic bacteria).[1–11] Furthermore, exciton transfer is exploited in the fluorescence resonance energy transfer (FRET) imaging technique that enables the tracking of individual molecules in living cells.[12–17]

In nanoscience, exciton dynamics have a crucial influence on the properties of numerous man-made materials. A prominent example are 2D materials, such as transition metal dichalcogenides, in which strongly bound excitons are responsible for their outstanding optical properties.[18–26] Organic optoelectronics, including organic light emitting diodes (OLEDs)[27–29] and organic solar cells (OSCs),[30–39] constitutes another vast field, which fundamentally relies on the properties of excitons.

The starting point of the theoretical description of intermolecular exciton transfer (also known as excitation energy transfer (EET)) is an electronically excited donor molecule D* and an acceptor molecule A in the ground state. The excitation energy is transferred from D* to A, leaving the donor in the ground state and the acceptor in the excited state (see Fig. 1). The rate at which this transfer proceeds is usually computed on the basis of Fermi's golden rule:[40,41]

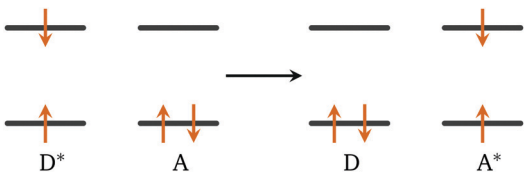

Fig. 1 MO scheme of singlet exciton transfer for a HOMO–LUMO excitation.

$$k_{\mathrm{EET}} = \frac{2\pi}{\hbar}|V_{\mathrm{DA}}|^2 J_{\mathrm{DA}},$$

where V_{DA} is the electronic coupling element between donor and acceptor, J_{DA} is the spectral overlap of the vibrationally resolved emission and absorption spectra, and $\hbar$ is the reduced Planck's constant. In the usual Condon approximation, V_{DA} is assumed not to depend explicitly on the nuclear coordinates. Effects due to nuclear motion are thus solely contained in J_{DA}.

In his pioneering work on EET, Förster expressed V_{DA} as the pure Coulomb coupling between the molecular dipoles of A and D.[40] Due to its simplicity and its applicability to many experimental scenarios, this approximation has been used extensively.[3,4,6,9,42–45] However, at small distances as, for instance, encountered in organic semiconductors and photovoltaics, the dipole approximation breaks down and the actual charge density distribution together with orbital overlap and exchange coupling has to be taken into account.[46–48] Within time-dependent density functional theory (TDDFT), transition densities are readily available, improving the accuracy of calculated Coulomb couplings.[9,11,49–51] However, as already

Institute of Solid State Theory and Center for Multiscale Theory and Computation, Westfälische Wilhelms-Universität Münster, 48149 Münster, Germany.
E-mail: nikos.doltsinis@wwu.de

† Electronic supplementary information (ESI) available. See DOI: 10.1039/c9cp06419b

proposed by Dexter,[52] neglect of exchange effects still leads to significant deviations at small distances, making more accurate approximations necessary at distances below about 6 Å.[53–57]

The calculation of coupling elements from the splitting of dimer excited states in TDDFT calculations further improves upon these methods, as the whole system is treated within a supermolecular approach.[11,58–60] While this technique includes Coulomb and exchange coupling as well as orbital overlap effects, its application is straightforward only in the case of homodimers, *i.e.* transfer between molecules of the same kind.[48] Mitigating also this shortcoming, the fragment excitation density (FED) method explicitly calculates coupling elements between localised exciton states and provides rates that compare well with experimental findings.[46,61–64]

Subotnik *et al.* have constructed diabatic localised exciton states *via* Boys orbital localisation, also enabling the direct evaluation of coupling matrix elements.[65–67] Notably, recent implementations of subsystem TDDFT allow the easy construction of diabatic localised exciton states[10,68–71] and the real-time sTDDFT formalism enables the direct simulation of transfer processes, even including nuclear dynamics, on short timescales.[72] Nevertheless, nuclear motion is overlooked in the vast majority of studies on exciton transfer. Most often, the spectral overlap J_{DA} is either completely neglected or obtained from experiments or simplified by assuming harmonic oscillations.[3,51,73–76] Zhang *et al.* have included explicit electron–phonon coupling in their Monte-Carlo simulations[77] and Plötz *et al.* have calculated coupling elements for geometries sampled from molecular dynamics (MD) simulations.[47] Recently, Londi *et al.* have used MD simulations to calculate semi-classical Marcus–Levich–Jortner rates.[78] On the whole, however, Fermi's golden rule and the Condon approximation are overwhelmingly adopted, although they are strictly only applicable in the weak coupling regime.[48,79]

The approach presented in this work circumvents those approximations, as it allows the direct evaluation of free energy barriers for exciton transfer from Car–Parrinello molecular dynamics, fully taking into account electronic and nuclear degrees of freedom. The excitonic electron–hole pair is represented by the singly occupied molecular orbitals (SOMOs) of the lowest excited singlet electronic state S_1, with the energetically lower orbital ($SOMO_h$) corresponding to the hole and the higher ($SOMO_e$) corresponding to the electron.

The exciton's position is defined by the centroid of maximally localised Wannier orbital centres corresponding to the SOMOs. The projection of the centroid position onto a reaction coordinate is then used to describe the transfer between two sites. In analogy to free energy calculations in classical MD, a restraining potential is applied to the Wannier centres, resulting in an additional force acting on the molecular orbitals in the Car–Parrinello equations of motion. An efficient implementation of these forces in the CPMD code[80] is presented and successfully tested.

Restraining the exciton position allows for classical free energy methods such as umbrella sampling to be employed. With these methods, even rare events become accessible, irrespective of their timescale. This technique is applied to model exciton transfer in poly(3-hexylthiophene), a common donor material in bulk-heterojunction organic solar cells.[38,39,81–87] The simulations show that the exciton position can indeed be controlled by the restraining potential. Moreover the calculated transition rates compare favourably with previously reported experimental diffusion constants.

2 Theory

In order to derive the forces arising from restraint potentials acting on Wannier centres, the key formulae regarding the definition of maximally localized Wannier orbitals and Wannier centres are briefly introduced.

2.1 Wannier orbitals in a plane wave basis

The Wannier orbital $|\boldsymbol{T}i\rangle$ for lattice vector $\boldsymbol{T}$ and band index i is defined as[88]

$$|\boldsymbol{T}i\rangle = \frac{\Omega}{(2\pi)^3}\int \mathrm{d}\boldsymbol{k}\, \mathrm{e}^{-\mathrm{i}\boldsymbol{k}\cdot\boldsymbol{T}}|\phi_{\boldsymbol{k}i}\rangle,$$

where Ω is the volume of the unit cell and the $|\phi_{\boldsymbol{k}i}\rangle$ are Bloch orbitals for wave vector $\boldsymbol{k}$. Defining the lattice periodic functions[89]

$$u_{\boldsymbol{k}i}(\boldsymbol{r}) = \mathrm{e}^{-\mathrm{i}\boldsymbol{k}\cdot\boldsymbol{r}}\phi_{\boldsymbol{k}i}(\boldsymbol{r}),$$

expectation values for operators $\hat{A}$ in the Wannier basis can be written as

$$\langle \boldsymbol{T}i|\hat{A}|\boldsymbol{0}j\rangle = \mathrm{i}\frac{\Omega}{(2\pi)^3}\int \mathrm{d}\boldsymbol{k}\, \mathrm{e}^{-\mathrm{i}\boldsymbol{k}\cdot\boldsymbol{T}}\langle u_{\boldsymbol{k}i}|\tilde{A}|u_{\boldsymbol{k}j}\rangle,$$

where $\hat{A}$ is the Fourier transform of $\hat{A}$. Based on this, the Wannier centres are defined as the expectation value of the position operator $\boldsymbol{r}$ within the unit cell at $\boldsymbol{T} = 0$:[90]

$$\langle \boldsymbol{r}_i\rangle = \langle \boldsymbol{0}i|\boldsymbol{r}|\boldsymbol{0}i\rangle = \mathrm{i}\frac{\Omega}{(2\pi)^3}\int \mathrm{d}\boldsymbol{k}\langle u_{\boldsymbol{k}i}|\boldsymbol{\nabla}_{\boldsymbol{k}}|u_{\boldsymbol{k}i}\rangle. \quad (1)$$

Maximally localised Wannier orbitals are obtained through minimisation of the total spread

$$\Theta = \sum_i \left(\langle r^2\rangle_i - \langle \boldsymbol{r}\rangle_i^2\right)$$

by applying a unitary transformation $\boldsymbol{U}(\boldsymbol{k})$ to the Wannier orbitals:

$$|u_{\boldsymbol{k}i}\rangle \rightarrow \sum_j U_{ji}(\boldsymbol{k})|u_{\boldsymbol{k}j}\rangle$$

The term Wannier centre then corresponds to the expectation value (1) in the maximally localised basis.

In practice, additional complications arise from the discretisation in reciprocal space. Vanderbilt *et al.* have derived an expression that maintains the translational properties of Wannier centres and their spread,[90] which for the Γ point and arbitrary cell geometry reduces to[91]

$$\langle r\rangle_i^{\alpha} = -\sum_{\beta}\frac{h_{\beta\alpha}}{2\pi}\mathrm{Im}\ln(\tilde{z}_{ii}^{\beta}) \quad (2)$$

where $h_{\beta\alpha}(\alpha, \beta = x, y, z)$ are elements of the matrix $\boldsymbol{h} = [\boldsymbol{a}_1,\boldsymbol{a}_2,\boldsymbol{a}_3]$ containing the lattice vectors $\boldsymbol{a}_i$. The matrix elements z_{ij}^{α} are given by

$$z_{ij}^{\alpha} = \int_{\Omega} \mathrm{d}\boldsymbol{r}\, \mathrm{e}^{\mathrm{i}\boldsymbol{g}_{\alpha}\cdot\boldsymbol{r}} \tilde{\phi}_i^*(\boldsymbol{r})\tilde{\phi}_j(\boldsymbol{r}),$$

with vectors $\boldsymbol{g}_{\alpha}$ defining the Cartesian components of the centre. The Kohn–Sham orbitals are transformed as well, leading to

$$|\phi_i\rangle \rightarrow |\tilde{\phi}_i\rangle = \sum_j U_{ji}|\phi_j\rangle \tag{3}$$

and thus

$$\tilde{z}_{ij}^{\alpha} = \sum_{kl} U_{ki}^{\dagger} U_{lj} z_{kl}^{\alpha}.$$

2.2 Restraining potentials

Next, the quantum-mechanical force resulting from a general potential V acting on a Wannier centre $\langle \boldsymbol{r}_i \rangle$ is derived. The centres $\langle \boldsymbol{r}_i \rangle$ themselves depend on the matrix elements $\tilde{z}_{ii}^{\beta}$, which, in turn, are functionals of all orbitals $\{\phi_j\}$:

$$V(\langle \boldsymbol{r}_i \rangle) = V(\langle \boldsymbol{r}_i \rangle\ (\tilde{z}_{ii}^{\beta}[\{\phi_j\}])). \tag{4}$$

The forces produced by the potential are thus functional derivatives with respect to the orbitals. The expression for those can be split into three terms by invoking the chain rule:

$$\begin{aligned} \frac{\delta V}{\delta \phi_j^*(\boldsymbol{r}')} &= \sum_{\alpha,i} \frac{\partial V}{\partial \langle r_\alpha \rangle_i} \cdot \frac{\delta \langle r_\alpha \rangle_i (\{\tilde{z}_{ii}^{\beta}\})}{\delta \phi_j^*(\boldsymbol{r}')} \\ &= \sum_{\alpha,\beta,i} \frac{\partial V}{\partial \langle r_\alpha \rangle_i} \cdot \frac{\partial \langle r_\alpha \rangle_i}{\partial \tilde{z}_{ii}^{\beta}} \cdot \frac{\delta \tilde{z}_{ii}^{\beta}}{\delta \phi_j^*(\boldsymbol{r}')}. \end{aligned} \tag{5}$$

The first term is, as for the classical analogue, the partial derivative of the potential with respect to the centre. For example, a harmonic potential

$$V(\langle \boldsymbol{r} \rangle_i) = \frac{K_{\mathrm{r}}}{2}(\langle \boldsymbol{r} \rangle_i - \boldsymbol{R}_0)^2$$

with force constant K_{r} and equilibrium position $\boldsymbol{R}_0$ yields

$$\frac{\partial V}{\partial \langle r_\alpha \rangle_i} = K_{\mathrm{r}}(\langle r_\alpha \rangle_i - R_{0\alpha}).$$

The second term of (5) is the partial derivative of the Wannier centre (2) with respect to the complex matrix element $\tilde{z}_{ii}^{\beta}$, which involves differentiation of the imaginary part of the complex logarithm $\mathrm{Im}\ln(z) = \arg(z)$ with respect to a complex number $z = r\mathrm{e}^{\mathrm{i}\varphi}$:

$$\frac{\partial}{\partial z}\mathrm{Im}\ln(z) = \left(\mathrm{e}^{-\mathrm{i}\varphi}\frac{\partial}{\partial r} - \frac{\mathrm{i}}{z}\frac{\partial}{\partial \varphi}\right)\arg(z) = -\frac{\mathrm{i}}{z}.$$

This leads to the expression

$$\frac{\partial \langle r_\alpha \rangle_i}{\partial \tilde{z}_{ii}^{\beta}} = \frac{h_{\alpha\beta}}{2\pi}\frac{\mathrm{i}}{\tilde{z}_{ii}^{\beta}}.$$

The last term of (5) is the functional derivative of the matrix element $\tilde{z}_{ii}^{\beta}$ with respect to the orbitals:

$$\begin{aligned} \frac{\delta \tilde{z}_{ii}^{\beta}}{\delta \phi_j^*(\boldsymbol{r}')} &= \frac{\delta}{\delta \phi_j^*(\boldsymbol{r}')} \sum_{k,l} U_{ki}^{\dagger} U_{li} \int_{\Omega} \mathrm{d}\boldsymbol{r}\, \mathrm{e}^{\mathrm{i}\boldsymbol{g}_{\beta}\cdot\boldsymbol{r}} \phi_k^*(\boldsymbol{r})\phi_l(\boldsymbol{r}) \\ &= \sum_{k,l} U_{ki}^{\dagger} U_{li} \int_{\Omega} \mathrm{d}\boldsymbol{r}\, \mathrm{e}^{\mathrm{i}\boldsymbol{g}_{\beta}\cdot\boldsymbol{r}} \delta_{kj}\delta(\boldsymbol{r} - \boldsymbol{r}')\phi_l(\boldsymbol{r}) \\ &= \sum_{l} U_{ji}^{\dagger} U_{li} \mathrm{e}^{\mathrm{i}\boldsymbol{g}_{\beta}\cdot\boldsymbol{r}} \phi_l(\boldsymbol{r}'). \end{aligned}$$

Combining these derivatives and using the short notation for the transformed orbitals (3), the final expression in real space is obtained:

$$\frac{\delta V}{\delta \phi_j^*(\boldsymbol{r})} = \frac{\mathrm{i}}{2\pi}\sum_i U_{ji}^{\dagger} \sum_{\alpha,\beta} \frac{\partial V}{\partial \langle r_\alpha \rangle_i} \frac{h_{\alpha\beta}}{\tilde{z}_{ii}^{\beta}} \mathrm{e}^{\mathrm{i}\boldsymbol{g}_{\beta}\cdot\boldsymbol{r}} \tilde{\phi}_i(\boldsymbol{r}). \tag{6}$$

This expression can be used for any potential $V(\langle \boldsymbol{r}_i \rangle)$, for which the partial derivative $\frac{\partial V}{\partial \langle r_\alpha \rangle_i}$ is known.

2.3 Implementation

In the CPMD code, the orbitals are stored as coefficients $C_j(\boldsymbol{G})$ in a plane-wave basis, where j is the orbital index and $\boldsymbol{G}$ is a reciprocal lattice vector. (Note that here we consider only the Γ-point approximation; however the formalism can be straightforwardly generalized.) Thus, the Fourier transform of the force (6) is implemented as

$$\frac{\delta V}{\delta C_j(\boldsymbol{G})} = \frac{\mathrm{i}}{2\pi}\sum_i U_{ji}^{\dagger} \sum_{\alpha,\beta} \frac{\partial V}{\partial \langle r_\alpha \rangle_i} \frac{h_{\alpha\beta}}{\tilde{z}_{ii}^{\beta}} \tilde{C}_i(\boldsymbol{G} + \boldsymbol{g}_{\beta}), \tag{7}$$

where the $\tilde{C}_i(\boldsymbol{G})$ are the transformed coefficients of the maximally localized Wannier orbitals:

$$\tilde{C}_i(\boldsymbol{G}) = \sum_j U_{ji} C_j(\boldsymbol{G}).$$

As the shifted coefficients $\tilde{C}_i(\boldsymbol{G} + \boldsymbol{g}_{\beta})$ as well as the transformation matrix $\boldsymbol{U}$ and the matrix elements $\tilde{z}_{ii}^{\beta}$ are determined anyway during the usual calculation of Wannier centres, the only overhead produced here is the evaluation of the force (7) itself.

In order to investigate the transfer of a Wannier centre from one molecule to another, an appropriate reaction coordinate needs to be defined. To this end, a general coordinate ξ defining a position $\boldsymbol{x} = \boldsymbol{A} + (\boldsymbol{B} - \boldsymbol{A})\cdot\xi$ on a line connecting two distinct groups of atoms is implemented (see Fig. 2).

With this, any position $\boldsymbol{x}$ can be projected onto a one-dimensional reaction coordinate ξ:

$$\xi = \frac{(\boldsymbol{B} - \boldsymbol{A}) \cdot (\boldsymbol{x} - \boldsymbol{A})}{|\boldsymbol{B} - \boldsymbol{A}|^2}. \tag{8}$$

Thus, $\xi = 0$ describes localisation on molecule A, while $\xi = 1$ means localisation on molecule B. A harmonic restraining

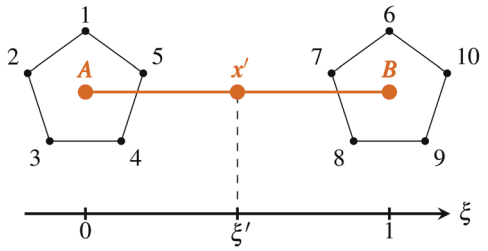

Fig. 2 Definition of the reaction coordinate ξ. ***A*** is the centre of mass (c.o.m.) of atoms 1–5, ***B*** is the c.o.m. of atoms 6–10. $\boldsymbol{x}'$ is the current position vector and ξ' the corresponding reaction coordinate according to eqn (8).

potential acting on ξ translates to

$$V(\xi) = \frac{K_\xi}{2}(\xi - \xi_{\mathrm{ref}})^2 = \frac{\tilde{K}_\xi}{2}(\boldsymbol{x} - \boldsymbol{x}_{\mathrm{ref}})^2 \tag{9}$$

where

$$\tilde{K}_\xi = \frac{K_\xi}{|\boldsymbol{B} - \boldsymbol{A}|^2} \tag{10}$$

and can be used to calculate the derivative in eqn (7). The 1D reaction coordinate ξ enables the application of known free energy techniques such as umbrella sampling. To model the transfer of an electron–hole pair, we choose not to restrain the two orbitals involved individually, but their centroid

$$\boldsymbol{x} = \frac{\langle \boldsymbol{r} \rangle_1 + \langle \boldsymbol{r} \rangle_2}{2} \tag{11}$$

The harmonic restraining potential (9) acting on this centroid then leads to the gradient

$$\frac{\partial V}{\partial \langle \boldsymbol{r} \rangle_i} = 2 \cdot \frac{\tilde{K}_\xi}{2}(\boldsymbol{x} - \boldsymbol{x}_{\mathrm{ref}}) \cdot \frac{\partial \boldsymbol{x}}{\partial \langle \boldsymbol{r} \rangle_1} = \frac{\tilde{K}_\xi}{2}(\langle \boldsymbol{r}_i \rangle - \boldsymbol{x}_{\mathrm{ref}}) \quad \text{for } i = 1, 2.$$

A sample input for the implementation in the CPMD code is available in the ESI.† Patches to CPMD version 3.15.1 or version 4.3, which add harmonic restraining potentials as defined here are available on request.

3 Computational details

The simulations are performed with an in-house modified version of the CPMD 3.15.1 package. Unless specified otherwise, all calculations employ the PBE density functional[92] with Grimme's D2 dispersion correction.[93] Norm-conserving Troullier–Martins pseudopotentials[94] are used with a plane-wave cutoff of E_{cut} = 70 Ry. Excited states are modelled within the restricted open-shell Kohn–Sham (ROKS) formalism.[95–97] The simulation boxes are chosen to have at least 7 Å of vacuum in every direction to avoid interaction between periodic images. The smallest possible box to accommodate the systems in all cases has the dimensions 28 Å × 19 Å × 16 Å. Prior to the dynamics simulations, wavefunctions are optimised to a gradient below 1×10^{-7} a.u. For the Car–Parrinello simulations,[98] a timestep Δt = 4 a.u. and a fictitious orbital mass μ = 400 a.u. are chosen. A Nosé–Hoover thermostat[99,100] with a resonance frequency of ω = 2500 cm^{-1} is used to keep the nuclei at an average temperature of T = 300 K. Structures and orbitals are visualised using VMD 1.9.2 with the internal Tachyon renderer.[101,102] For orbitals obtained from CPMD properties calculations, an iso-value of 5 is used.

4 Results and discussion

4.1 Investigated molecules

As a model for the frequently used donor material in bulk-heterojunction solar cells, poly(3-hexylthiophene) (P3HT, see Fig. 3(left)),[38,39,81–87] we investigate penta(3-methylthiophene) (P3MT, see Fig. 3(right)), which has a chain length of n = 5 and the hexyl chains present in P3HT have been replaced by methyl groups.

Within ROKS, the first excited singlet state S_1 is approximated by a symmetry-adapted linear combination of two open-shell Slater determinants comprising a single set of molecular orbitals.

In Fig. 4a, the two SOMOs of a single P3MT molecule are presented, showing that the S_1 excitation has $\pi \rightarrow \pi^*$ character. The vertical excitation energy at the optimised S geometry is ΔE = 1.80 eV with the PBE functional. This result is lower than literature results for oligomers with chain lengths of 4 to 6, ranging from 2.49 eV to 2.96 eV in TDDFT calculations and from 2.85 eV to 3.16 eV in experiments.[86] On the other hand, the PBE value is quite close to experimental results of ~2.0 eV obtained for crystals.[86]

However, it is well known that ROKS generally underestimates excitation energies when used with GGA functionals – especially for $\pi \rightarrow \pi^*$ excitations.[103–110] For this reason, we implement the ROKS method with hybrid functionals yielding much improved excitation energies (see ESI† for details). As a matter of fact, ROKS calculations

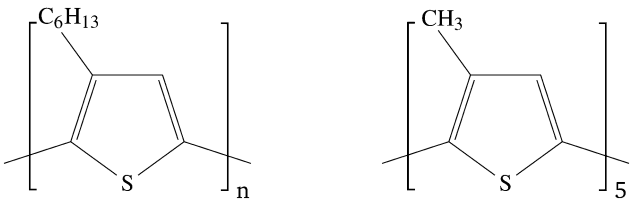

Fig. 3 Structures of poly(3-hexylthiophene) (left) and penta(3-methylthiophene) (right).

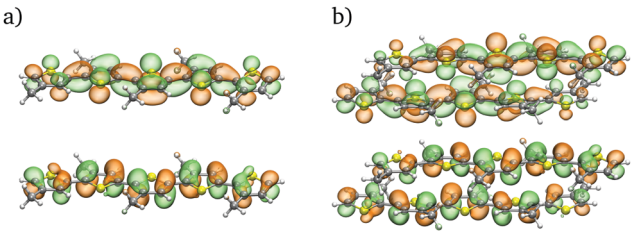

Fig. 4 $SOMO_e$ (top) and $SOMO_h$ (bottom) of a P3MT monomer (a) and Di-P3MT (b) obtained from ROKS calculations at the respective optimized ground state geometries.

with the PBE0 hybrid functional[111,112] (at the PBE geometry) yield an excitation energy of 2.30 eV for P3MT, *i.e.* 0.5 eV higher than with PBE. Since the calculation of the exact exchange energy in a plane-wave basis is, however, considerably more time-consuming, the dynamics simulations in this work are performed with the GGA functional PBE. The shape of the GGA-ROKS potential energy surfaces has been shown to be comparable to that obtained with more accurate methods – including CASPT2 and TDDFT.[104–110] This observation has been specifically made for $\pi \rightarrow \pi^*$ excited states in numerous different molecules leading to realistic excited state dynamics in agreement with experimental observations.

In the following, we refer to a single P3MT molecule as a monomer. In order to simulate intermolecular exciton transfer, a dimer (Di-P3MT) is constructed by rotating a second monomer by 180° and laying it on top of the other, with the aromatic rings parallel to each other, as shown in Fig. 5. To keep the monomers at a certain distance, intermolecular restraining potentials are used throughout the simulations. In particular, the intermolecular distance d is defined as the distance of the sulfur atom of each ring of one monomer to the middle of the C–C bond of the corresponding ring on the other monomer (see Fig. 5) as these points practically lie on top of each other in the optimized geometry. To realize a certain value of d, harmonic potentials with a force constant of $K_{\mathrm{bond}} = 0.1$ a.u. are applied between the sulfur atom of each ring of monomer A (B) and the corresponding two carbon atoms of monomer B (A), restraining the distance $d' = \sqrt{d^2 + d_{\mathrm{C-C}}{}^2}$ (see Fig. 5). Here, $d_{\mathrm{C-C}} = 1.4$ Å is the length of the C–C bond, which leads to the restrained distances d' specified in Table S2 (ESI†). This way, to restrain the intermolecular distance d, in total 20 restraints are applied (4 to each pair of aromatic rings) to the system. This additionally prevents the monomers from drifting apart in the direction of the chain, which otherwise occurs in longer unrestrained simulations due to the shortened chain length (see Fig. S1 and S2, ESI†), but is largely absent in real condensed phases.

For the S_1 excited state of the dimer, the SOMOs now correspond to linear combinations of the monomer SOMOs (see Fig. 1b). This leads to a lower excitation energy of $\Delta E = 1.60$ eV with the PBE functional and $\Delta E = 2.15$ eV with the PBE0 functional.

4.2 Free exciton dynamics

First, the character of the exciton in the Di-P3MT model system is examined by performing a Car–Parrinello simulation in the S_1 state without any restraints whatsoever – *i.e.* neither Wannier centres nor nuclear positions are restrained. During the simulation time of 2 ps, Wannier centres are calculated for the SOMOs at each timestep and an exciton coordinate ξ is calculated *via* formulae (8) and (11), placing the vectors $\boldsymbol{A}$ and $\boldsymbol{B}$ (see also Fig. 2) at the c.o.m. of the central thiophene ring (considering the four carbons and the sulfur atom) of each P3MT monomer. The resulting time evolution of the exciton coordinate is shown in Fig. 6.

The exciton is localised mostly on monomer B ($\xi = 1$), with occasional jumps to monomer A ($\xi = 0$). This indicates that the exciton transfer in Di-P3MT can be described as a hopping process of a localised Frenkel exciton from an excited Donor D* to an acceptor A (see Fig. 1). Denoting the initial state as $|\mathrm{D^*A}\rangle$ and the final state as $|\mathrm{DA^*}\rangle$, the wavefunction of the Frenkel exciton can be written as

$$|\Psi\rangle = c_1|\mathrm{D^*A}\rangle + c_2|\mathrm{DA^*}\rangle.$$

With $\langle\Psi|\Psi\rangle = 1$ it is obvious that $c_2 = \sqrt{1 - c_1{}^2}$, leaving one degree of freedom describing the transfer process. As shown in Fig. 7, both SOMOs are fully localised on one monomer for $\xi = 0$ and $\xi = 1$. For $\xi = 0.5$, however, both SOMOs exhibit localisation on both monomers, corresponding to a Frenkel exciton with the wavefunction

$$|\Psi\rangle = \frac{1}{\sqrt{2}}|\mathrm{D^*A}\rangle + \frac{1}{\sqrt{2}}|\mathrm{DA^*}\rangle.$$

This further indicates that ξ is a viable reaction coordinate, which can be interpreted as the localisation of a Frenkel exciton $\xi = c_1{}^2$.

4.3 Restraining potentials

As illustrated by Fig. 6, the exciton in Di-P3MT is predominantly localised on one of the monomers, *i.e.* $\xi = 0$ or $\xi = 1$, especially at large intermolecular separations. To calculate the free energy barrier for intermolecular exciton transfer – for instance, using umbrella sampling – a suitable restraining

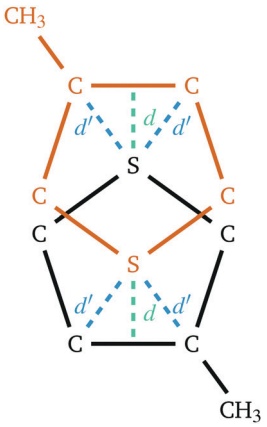

Fig. 5 Definition of the intermolecular distance d.

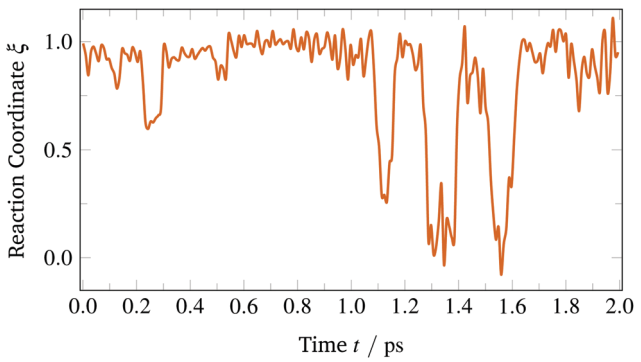

Fig. 6 Time evolution of the exciton coordinate ξ from an unrestrained simulation of Di-P3MT over 2 ps.

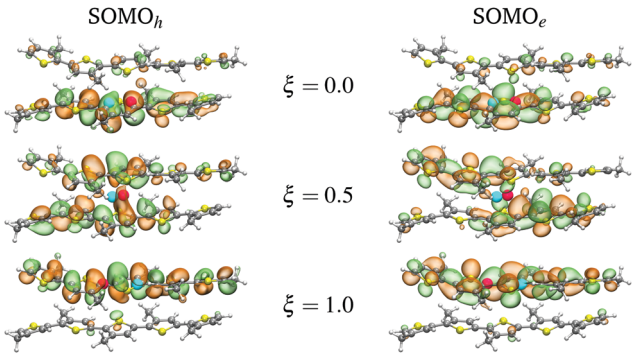

Fig. 7 Snapshots of the SOMOs corresponding to hole and electron from a dimer simulation without restraints. The Wannier centres of the hole and electron states are shown as a blue and red spheres, respectively.

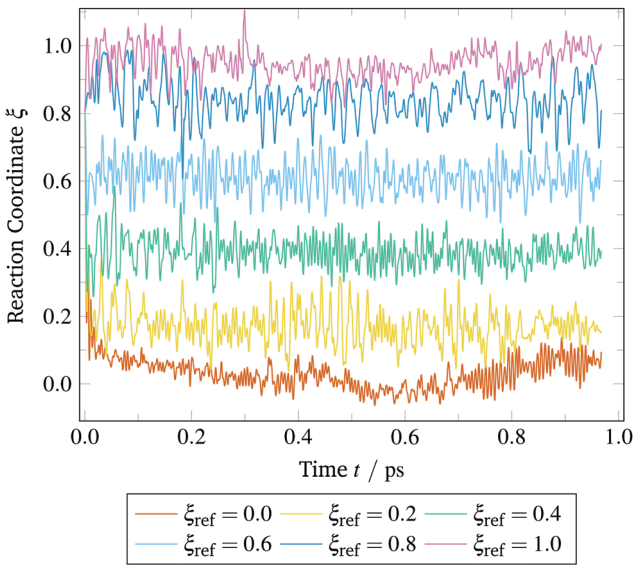

Fig. 8 Exciton coordinate during an MD simulation of Di-P3MT at d = 4.0 Å with a harmonic restraining potential with force constant K_ξ = 0.3 a.u. keeping the exciton centre close to the reference coordinate ξ_{ref}.

potential needs to be applied that connects initial and final states and is able to keep the exciton coordinate close to any predefined value along the reaction path. Fig. 8 shows the time-evolution of the actual exciton coordinate ξ for different reference values ξ_{ref} specified in the harmonic potential (9).

The harmonic potential clearly keeps the exciton fairly close to the specified position for all reference values and is thus able to control exciton transfer. The amplitude of the oscillations can be controlled by the force constant K_ξ, as shown in Fig. 9 and Fig. S3 (ESI†).

Application of restraining potentials on the orbital positions obviously leads to an increase in fictitious electronic kinetic energy (see Fig. S4, ESI†), as additional oscillations are induced. Since the harmonic potential (9) acts on an orbital with fictitious mass μ, it will oscillate with the frequency

$$\omega = \sqrt{\frac{\tilde{K}_\xi}{\mu}}.$$

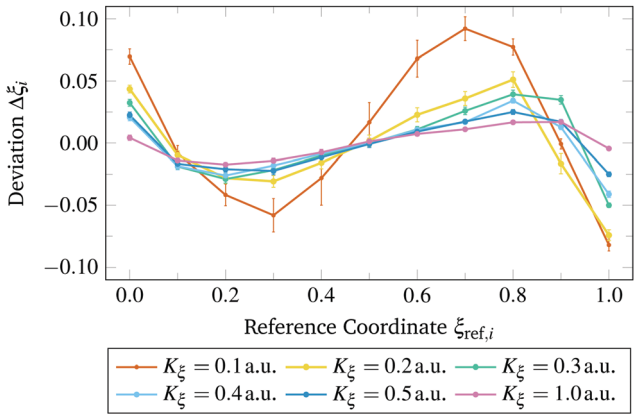

Fig. 9 Deviation of the average exciton coordinate from the reference, *i.e.* $\Delta\xi_i = \xi_i - \xi_{ref,i}$ for different force constants K_ξ and windows i. The error bars correspond to one standard deviation σ_i.

For example, an intermolecular distance of $|\boldsymbol{B} - \boldsymbol{A}| = d$ = 4.0 Å, a force constant of K_ξ = 0.2 a.u. (corresponding to $\tilde{K}_\xi$ = 0.34 eV Å^{-2}), and a fictitious orbital mass of μ = 400 a.u., lead to a frequency of ω = 4079 cm^{-1}. Since this value is close to the range of the nuclear vibrational frequencies (see Fig. S5, ESI†), electronic and nuclear degrees of freedom are not completely decoupled, causing the Car–Parrinello method to break down as energy is transferred from the nuclear to the electronic subsystem. Therefore, an additional Nosé–Hoover thermostat is applied to the orbital degrees of freedom. The kinetic energy is kept constant corresponding to the temperature $T = 2k_B\langle E_{kin,el}\rangle/N_{DOF}$ = 300 K. Here N_{DOF} is the number of electronic degrees of freedom and is equivalent to the number of orbitals. In the case of Di-P3MT, N_{DOF} = 153 resulting in $\langle E_{kin,el}\rangle$ = 0.073 a.u.

4.4 Umbrella sampling and free energies

Having shown that the chosen restraint is capable of keeping the exciton coordinate within small windows along the reaction coordinate with controllable deviation, we now employ this method to calculate free energy barriers for exciton transfer within the framework of umbrella sampling.[113–115] Average forces, *i.e.* the partial derivative of the free energy F_i w.r.t. ξ, $\frac{\partial F_i}{\partial \xi}$, are obtained by umbrella integration from the average coordinate $\langle\xi_i\rangle$ and its standard deviation σ_i for each window i:

$$\frac{\partial F_i}{\partial \xi} = \frac{1}{\beta}\frac{\xi - \langle\xi_i\rangle}{\sigma_i^2} - K_\xi(\xi - \xi_i^{ref}),$$

with $\beta = (k_B T)^{-1}$, where k_B is the Boltzmann constant and T is the temperature. The total force $\frac{\partial F}{\partial \xi}$ is then the weighted sum over the forces of the windows:

$$\frac{\partial F}{\partial \xi} = \sum_i p_i(\xi)\frac{\partial F_i}{\partial \xi},$$

with the weights defined by Gaussian distributions:

$$p_i(\xi) = \frac{a_i(\xi)}{\sum_j a_j(\xi)}$$

$$a_i(\xi) = N_i P_i(\xi),$$

$$P_i(\xi) = \frac{1}{\sigma_i\sqrt{2\pi}} \exp\left[-\frac{1}{2}\left(\frac{\xi - \langle\xi_i\rangle}{\sigma_i}\right)^2\right],$$

for the number of simulation steps N_i. The thus obtained average force is then integrated on a grid of 1000 ξ-values between $\xi = 0$ and $\xi = 1$.

In the following, a force constant of $K_\xi = 0.2$ a.u. is used in order to have sufficient overlap between the 11 equally spaced windows $\xi_{\mathrm{ref},i} = n{\cdot}0.1$ ($n = 0, 1, \ldots, 10$). Due to the symmetry of the Di-P3MT model system, the free energy curves are expected to be symmetric around $\xi = 0.5$. Deviations, most noticeable for $d = 4.5$ Å and $d = 5.0$ Å (see Fig. 10), arise from asymmetric dynamics of the monomers and can ultimately be attributed to the fact that simulation times are finite. In the thermodynamic limit, all configurations would be sampled and the curves would be symmetric. Nevertheless, the curves show a clear trend: the farther the monomers are apart, the higher the barrier for exciton transfer. This result is expected from the known exponential distance dependence of the Dexter energy transfer rate.[52]

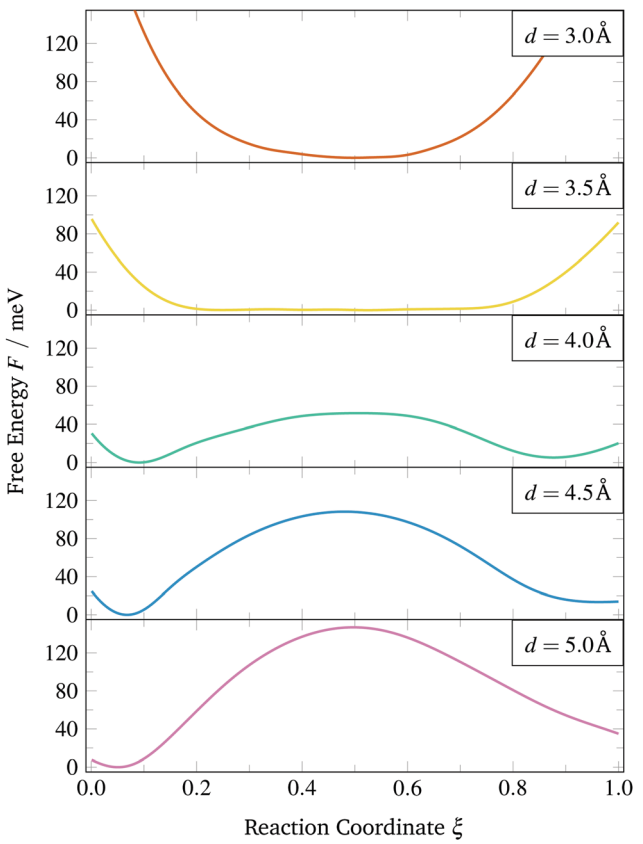

Fig. 10 Free energy profiles for the exciton transfer between two P3MT monomers at intermolecular distances of (from top to bottom) $d = 3.0$ Å, $d = 3.5$ Å, $d = 4.0$ Å, $d = 4.5$ Å and $d = 5.0$ Å.

To assess whether these barriers are physically meaningful, transfer rates and diffusion constants are estimated from the barrier heights and compared to experimental results.

According to transition state theory, the rates can be estimated from transmissivity κ and the probability to reach the transition state, *i.e.* the maximum ξ^*:[116–118]

$$P(\xi^*) = \frac{\exp[-\beta F(\xi^*)]}{\int_{-\infty}^{\xi^*} \exp[-\beta F(\xi)]\mathrm{d}\xi}$$

The transmissivity κ accounts for the dynamics at the maximum and can be calculated from the average velocity at the maximum

$$\kappa = \langle\dot{\xi}\Theta(\dot{\xi})\rangle_{\xi=\xi^*},$$

where the Heaviside function $\Theta(\dot{\xi})$ ensures that only positive velocities are counted as only those correspond to the exciton crossing the barrier. The velocity of the exciton coordinate $\dot{\xi}$ is readily available from the restrained simulations at the maximum of the barrier. Note that, in contrast to constraints, restraining potentials do not influence expectation values of an arbitrary function f of the momentum within the canonical ensemble, as the integrals over momentum and position are separable

$$\begin{aligned}\langle f(\boldsymbol{p})\rangle &= \frac{1}{Z}\int_{\mathbb{R}} \mathrm{d}\boldsymbol{r}\int_{\mathbb{R}} \mathrm{d}\boldsymbol{p}\, f(\boldsymbol{p}) \exp\left[-\beta\frac{\boldsymbol{p}^2}{2m} - \beta V(\boldsymbol{r})\right] \\ &= \frac{1}{Z}\int_{\mathbb{R}} \mathrm{d}\boldsymbol{r} \exp[-\beta V(\boldsymbol{r})] \cdot \int_{\mathbb{R}} \mathrm{d}\boldsymbol{p}\, f(\boldsymbol{p}) \exp\left[-\beta\frac{\boldsymbol{p}^2}{2m}\right].\end{aligned}$$

Here, $\boldsymbol{p} = \mu\dot{\boldsymbol{x}}$ and, according to eqn (8), $\dot{\xi} = \frac{(\boldsymbol{B}-\boldsymbol{A})\cdot\boldsymbol{p}}{\mu|\boldsymbol{B}-\boldsymbol{A}|^2}$. This means that restrained simulations are perfectly suited for the calculation of the average velocity $\langle\dot{\xi}\Theta(\dot{\xi})\rangle_{\xi=\xi^*}$. In conjunction with the probability density $P(\xi^*)$, the exciton transfer rate can then be calculated as

$$k_{\mathrm{EET}} = \kappa P(\xi^*) = \langle\dot{\xi}\Theta(\dot{\xi})\rangle_{\xi=\xi^*} \frac{\exp[-\beta F(\xi^*)]}{\int_{-\infty}^{\xi^*} \exp[-\beta F(\xi)]\mathrm{d}\xi}.$$

We note that recrossings are not taken into account within transition state theory, *i.e.* particles which cross the barrier with a positive velocity are assumed to always reach the product state. As recrossings do occur in the investigated system (see Fig. 6), the rate calculated this way is always an upper limit to the exact transition rate.[119] More accurate methods, such as the Bennet–Chandler approach,[116,120] are, in principle, also accessible with our implementation. However, such approaches usually involve explicit simulations of recrossings, rendering the evaluation of recrossing rates with statistical significance computationally extremely demanding.

Further assuming a simple 1D random walk to approximate an ideal P3MT crystal, diffusion constants follow from[121]

$$D = \frac{(\Delta x)^2}{2\Delta t},$$

Table 1 Free energy barriers ΔF, transfer rates k_{EET} and diffusion constants D for Di-P3MT for different intermolecular distances d. For d = 3.0 Å, no rates and diffusion constants can be calculated

d/Å	ΔF/meV	k_{EET}/ps^{-1}	D/10^{-3} cm^2 s^{-1}
3.0	0.00	—	—
3.5	0.93	1844.13	1129.53
4.0	51.63	27.43	21.95
4.5	108.28	5.31	5.37
5.0	146.89	0.71	0.89

where the hopping distance Δx corresponds to the intermolecular distance d and the hopping time Δt is the inverse of the exciton transfer rate k_{EET}. This finally leads to

$$D = \frac{d^2 \cdot k_{EET}}{2}.$$

The barrier heights, transfer rates, and diffusion constants obtained in this way are collected in Table 1. For $d < 4.0$ Å, the barrier practically vanishes, so the given rates and diffusion constants are only meaningful for $d \geq 4.0$ Å.

While the applied approximations and model assumptions certainly do not represent the situation in real organic solar cells, they are fairly close to the limiting case of an ideal crystal. Indeed, the calculated diffusion constants agree surprisingly well with measurements conducted on P3HT crystals where values of $D = 3.3 \times 10^{-3}$ cm^2 s^{-1} and $D = 7.9 \times 10^{-3}$ cm^2 s^{-1} were found for low and high crystallinity, respectively.[38] According to the calculated diffusion constants, this would correspond to an intermolecular distance between d = 4.0 Å and d = 5.0 Å. Indeed, experiments report distances between d = 4.17 Å and d = 4.45 Å.[122,123] For amorphous P3HT crystals, reported diffusion constants vary strongly, ranging from $D = 0.5 \times 10^{-3}$ cm^2 s^{-1} to $D = 10 \times 10^{-3}$ cm^2 s^{-1}.[124–126] It can thus be concluded that the barriers obtained from umbrella sampling with restrained Wannier centres of the SOMOs make physical sense and do not contradict experimental measurements. A more meaningful comparison between theory and experiment requires more intricate models that include the actual crystal structure or morphology, *e.g.* by sampling from large-scale force field molecular dynamics simulations of P3HT crystals or by including further monomers or a surrounding environment in the simulation box. Beyond that, rates calculated for dimers could, as has been done for charge transfer rates,[127] be included in kinetic Monte-Carlo simulations for a larger box in order to analyse the exciton transfer efficiency of realistic solar cell architectures.

5 Conclusion

In this work, the theoretical framework and computational intricacies of Car–Parrinello molecular dynamics with restrained Wannier centres was presented. A technical implementation of the method in the CPMD program was successfully tested and the restraint approach was confirmed to be capable of effectively controlling the position of molecular orbitals along a predefined reaction coordinate. The new method was applied to compute free energy curves *via* umbrella sampling for exciton hopping between two stacked penta(3-methylthiophene) monomers. Effects due to nuclear motion, which are often neglected in alternative approaches, are fully taken into account. Exciton transition rates and diffusion constants obtained from this approach have been shown to be physically meaningful, as they compare well with experiments.

All in all, this work establishes restraining potentials acting on Wannier centres as novel and useful technique in the toolbox of *ab initio* molecular dynamics simulations. While the discussion here focuses on exciton transfer in organic semiconductors, this technique is generally applicable to any system. In particular, not only exciton transfer, but transfer of any kind of charge carriers can be envisioned to be investigated in this manner.

Conflicts of interest

There are no conflicts to declare.

Acknowledgements

This work was funded by the German Research Foundation (DFG) within SFB 858, TRR 61, and DO 768/4-1. Calculations were performed on the PALMA II HPC cluster of WWU Münster.

Notes and references

1 W. Kühlbrandt, D. N. Wang and Y. Fujiyoshi, *Nature*, 1994, **367**, 614–621.
2 T. Pullerits and V. Sundström, *Acc. Chem. Res.*, 1996, **29**, 381.
3 T. Pullerits, M. Chachisvilis and V. Sundström, *J. Phys. Chem.*, 1996, **100**, 10787.
4 X. Hu, T. Ritz, A. Damjanović and K. Schulten, *J. Phys. Chem. B*, 1997, **101**, 3854.
5 M. Chachisvilis, O. Kühn, T. Pullerits and V. Sundström, *J. Phys. Chem. B*, 1997, **101**, 7275.
6 V. Sundström, T. Pullerits and R. van Grondelle, *J. Phys. Chem. B*, 1999, **103**, 2327.
7 T. Renger, V. May and O. Kühn, *Phys. Rep.*, 2001, **343**, 137.
8 A. Damjanović, I. Kosztin, U. Kleinekathöfer and K. Schulten, *Phys. Rev. E: Stat., Nonlinear, Soft Matter Phys.*, 2002, **65**, 031919.
9 M. E. Madjet, A. Abdurahman and T. Renger, *J. Phys. Chem. B*, 2006, **110**, 17268.
10 C. König and J. Neugebauer, *Phys. Chem. Chem. Phys.*, 2011, **13**, 10475.
11 C. König and J. Neugebauer, *ChemPhysChem*, 2012, **13**, 386.
12 W. E. Moerner and L. Kador, *Phys. Rev. Lett.*, 1989, **62**, 2535.
13 E. Betzig, *Opt. Lett.*, 1995, **20**, 237.
14 T. A. Klar and S. W. Hell, *Opt. Lett.*, 1999, **24**, 954.
15 C. J. Weijer, *Science*, 2003, **300**, 96.
16 D. J. Stephens and V. J. Allan, *Science*, 2003, **300**, 82.

17 W. E. Moerner and D. P. Fromm, *Rev. Sci. Instrum.*, 2003, **74**, 3597.
18 K. F. Mak, C. Lee, J. Hone, J. Shan and T. F. Heinz, *Phys. Rev. Lett.*, 2010, **105**, 136805.
19 M. Palummo, M. Bernardi and J. C. Grossman, *Nano Lett.*, 2015, **15**, 2794.
20 I. Niehues, R. Schmidt, M. Drüppel, P. Marauhn, D. Christiansen, M. Selig, G. Berghäuser, D. Wigger, R. Schneider, L. Braasch, R. Koch, A. Castellanos-Gomez, T. Kuhn, A. Knorr, E. Malic, M. Rohlfing, S. Michaelis de Vasconcellos and R. Bratschitsch, *Nano Lett.*, 2018, **18**, 1751.
21 Y. Yu, A. W. Bataller, R. Younts, Y. Yu, G. Li, A. A. Puretzky, D. B. Geohegan, K. Gundogdu and L. Cao, *ACS Nano*, 2019, **13**, 10351.
22 V. Shahnazaryan, O. Kyriienko and H. Rostami, *Phys. Rev. B*, 2019, **100**, 165303.
23 M. Amani, D.-H. Lien, D. Kiriya, J. Xiao, A. Azcatl, J. Noh, S. R. Madhvapathy, R. Addou, S. KC, M. Dubey, K. Cho, R. M. Wallace, S.-C. Lee, J.-H. He, J. W. Ager, X. Zhang, E. Yablonovitch and A. Javey, *Science*, 2015, **350**, 1065.
24 H.-V. Han, A.-Y. Lu, L.-S. Lu, J.-K. Huang, H. Li, C.-L. Hsu, Y.-C. Lin, M.-H. Chiu, K. Suenaga, C.-W. Chu, H.-C. Kuo, W.-H. Chang, L.-J. Li and Y. Shi, *ACS Nano*, 2016, **10**, 1454.
25 C. Schwermann, T. Stiehm, P. Tonndorf, R. Schneider, R. Schmidt, J. Kern, S. Michaelis de Vasconcellos, R. Bratschitsch and N. L. Doltsinis, *Phys. Chem. Chem. Phys.*, 2018, **20**, 16918.
26 Y. Garcia-Basabe, G. G. Parra, M. B. Barioni, C. D. Mendoza, F. C. Vicentin and D. G. Larrud'e, *Phys. Chem. Chem. Phys.*, 2019, **21**, 23521.
27 M. A. Baldo, D. F. O'Brien, Y. You, A. Shoustikov, S. Sibley, M. E. Thompson and S. R. Forrest, *Nature*, 1998, **395**, 151.
28 A. Adronov and J. M. J. Fréchet, *Chem. Commun.*, 2000, 1701.
29 Y. Sun, N. C. Giebink, H. Kanno, B. Ma, M. E. Thompson and S. R. Forrest, *Nature*, 2006, **440**, 908.
30 C. J. Brabec, A. Cravino, D. Meissner, N. S. Sariciftci, T. Fromherz, M. T. Rispens, L. Sanchez and J. C. Hummelen, *Adv. Funct. Mater.*, 2001, **11**, 374.
31 M. Grätzel, *J. Photochem. Photobiol., C*, 2003, **4**, 145.
32 P. Peumans, A. Yakimov and S. R. Forrest, *J. Appl. Phys.*, 2003, **93**, 3693.
33 K. M. Coakley and M. D. McGehee, *Chem. Mater.*, 2004, **16**, 4533.
34 A. Hadipour, B. de Boer, J. Wildeman, F. B. Kooistra, J. C. Hummelen, M. G. R. Turbiez, M. M. Wienk, R. A. J. Janssen and P. W. M. Blom, *Adv. Funct. Mater.*, 2006, **16**, 1897.
35 S.-B. Rim, R. F. Fink, J. C. Schöneboom, P. Erk and P. Peumans, *Appl. Phys. Lett.*, 2007, **91**, 173504.
36 P. Blom, V. Mihailetchi, L. Koster and D. Markov, *Adv. Mater.*, 2007, **19**, 1551.
37 M. Scharber and N. Sariciftci, *Prog. Polym. Sci.*, 2013, **38**, 1929.
38 Y. Tamai, H. Ohkita, H. Benten and S. Ito, *J. Phys. Chem. Lett.*, 2015, **6**, 3417.
39 T. Winands, M. Böckmann, T. Schemme, P.-M. T. Ly, D. H. de Jong, Z. Wang, C. Denz, A. Heuer and N. L. Doltsinis, *Phys. Chem. Chem. Phys.*, 2016, **18**, 6217.
40 T. Förster, *Ann. Phys.*, 1948, **437**, 55.
41 V. May and O. Kühn, *Charge and Energy Transfer Dynamics in Molecular Systems*, John Wiley & Sons, Ltd, 2011.
42 K. Sauer, R. J. Cogdell, S. M. Prince, A. Freer, N. W. Isaacs and H. Scheer, *Photochem. Photobiol.*, 1996, **64**, 564.
43 H. van Amerongen and R. van Grondelle, *J. Phys. Chem. B*, 2001, **105**, 604.
44 S. C. J. Meskers, J. Hübner, M. Oestreich and H. Bässler, *J. Phys. Chem. B*, 2001, **105**, 9139.
45 C. Madigan and V. Bulović, *Phys. Rev. Lett.*, 2006, **96**, 046404.
46 K.-L. Liu, S.-J. Lee, I.-C. Chen, C.-P. Hsu, M.-Y. Yeh and T.-Y. Luh, *J. Phys. Chem. C*, 2010, **114**, 13909.
47 P.-A. Plötz, T. Niehaus and O. Kühn, *J. Chem. Phys.*, 2014, **140**, 174101.
48 Z.-Q. You and C.-P. Hsu, *Int. J. Quantum Chem.*, 2014, **114**, 102.
49 J. Guthmuller, F. Zutterman and B. Champagne, *J. Chem. Phys.*, 2009, **131**, 154302.
50 D. Ambrosek, H. Marciniak, S. Lochbrunner, J. Tatchen, X.-Q. Li, F. Würthner and O. Kühn, *Phys. Chem. Chem. Phys.*, 2011, **13**, 17649.
51 D. Ambrosek, A. Köhn, J. Schulze and O. Kühn, *J. Phys. Chem. A*, 2012, **116**, 11451.
52 D. L. Dexter, *J. Chem. Phys.*, 1953, **21**, 836.
53 S. Hassoon, H. Lustig, M. B. Rubin and S. Speiser, *J. Phys. Chem.*, 1984, **88**, 6367.
54 G. D. Scholes and K. P. Ghiggino, *J. Phys. Chem.*, 1994, **98**, 4580.
55 S. Faure, C. Stern, R. Guilard and P. D. Harvey, *J. Am. Chem. Soc.*, 2004, **126**, 1253.
56 J. A. Mondal, G. Ramakrishna, A. K. Singh, H. N. Ghosh, M. Mariappan, B. G. Maiya, T. Mukherjee and D. K. Palit, *J. Phys. Chem. A*, 2004, **108**, 7843.
57 S. W. Clark, J. M. Harbold and F. W. Wise, *J. Phys. Chem. C*, 2007, **111**, 7302.
58 A. H. A. Clayton, G. D. Scholes, K. P. Ghiggino and M. N. Paddon-Row, *J. Phys. Chem.*, 1996, **100**, 10912.
59 D. Beljonne, J. Cornil, R. Silbey, P. Millié and J. L. Brédas, *J. Chem. Phys.*, 2000, **112**, 4749.
60 M. P. Eng and B. Albinsson, *Angew. Chem., Int. Ed.*, 2006, **45**, 5626.
61 M. Head-Gordon, A. M. Grana, D. Maurice and C. A. White, *J. Phys. Chem.*, 1995, **99**, 14261.
62 H.-C. Chen, Z.-Q. You and C.-P. Hsu, *J. Chem. Phys.*, 2008, **129**, 084708.
63 A. A. Voityuk, *Phys. Chem. Chem. Phys.*, 2010, **12**, 7403.
64 S. R. Yost, E. Hontz, S. Yeganeh and T. Van Voorhis, *J. Phys. Chem. C*, 2012, **116**, 17369.
65 J. E. Subotnik, S. Yeganeh, R. J. Cave and M. A. Ratner, *J. Chem. Phys.*, 2008, **129**, 244101.
66 J. E. Subotnik, R. J. Cave, R. P. Steele and N. Shenvi, *J. Chem. Phys.*, 2009, **130**, 234102.
67 J. E. Subotnik, J. Vura-Weis, A. J. Sodt and M. A. Ratner, *J. Phys. Chem. A*, 2010, **114**, 8665.
68 A. Krishtal, D. Sinha, A. Genova and M. Pavanello, *J. Phys.: Condens. Matter*, 2015, **27**, 183202.

69 A. Krishtal and M. Pavanello, *J. Chem. Phys.*, 2016, **144**, 124118.
70 P. Ramos and M. Pavanello, *Phys. Chem. Chem. Phys.*, 2016, **18**, 21172.
71 D. G. Artiukhin and J. Neugebauer, *J. Chem. Phys.*, 2018, **148**, 214104.
72 A. Krishtal, D. Ceresoli and M. Pavanello, *J. Chem. Phys.*, 2015, **142**, 154116.
73 E. Hennebicq, G. Pourtois, G. D. Scholes, L. M. Herz, D. M. Russell, C. Silva, S. Setayesh, A. C. Grimsdale, K. Müllen, J.-L. Brédas and D. Beljonne, *J. Am. Chem. Soc.*, 2005, **127**, 4744.
74 S. Athanasopoulos, E. Hennebicq, D. Beljonne and A. B. Walker, *J. Phys. Chem. C*, 2008, **112**, 11532.
75 B. Van Averbeke and D. Beljonne, *ChemPhysChem*, 2009, **10**, 3061.
76 M. E. Köse, P. Graf, N. Kopidakis, S. E. Shaheen, K. Kim and G. Rumbles, *ChemPhysChem*, 2009, **10**, 3285.
77 X. Zhang, Z. Li and G. Lu, *Phys. Rev. B: Condens. Matter Mater. Phys.*, 2011, **84**, 235208.
78 G. Londi, R. Dilmurat, G. D'Avino, V. Lemaur, Y. Olivier and D. Beljonne, *Phys. Chem. Chem. Phys.*, 2019, advance article.
79 W. Liu, V. Settels, P. H. P. Harbach, A. Dreuw, R. F. Fink and B. Engels, *J. Comput. Chem.*, 2011, **32**, 1971.
80 *CPMD*, http://www.cpmd.org/, Copyright IBM Corp 1990–2019, Copyright MPI für Festkörperforschung Stuttgart 1997–2001.
81 L. Blinov, S. Palto, G. Ruani, C. Taliani, A. Tevosov, S. Yudin and R. Zamboni, *Chem. Phys. Lett.*, 1995, **232**, 401.
82 P. J. Brown, D. S. Thomas, A. Köhler, J. S. Wilson, J.-S. Kim, C. M. Ramsdale, H. Sirringhaus and R. H. Friend, *Phys. Rev. B: Condens. Matter Mater. Phys.*, 2003, **67**, 064203.
83 G. Li, V. Shrotriya, J. Huang, Y. Yao, T. Moriarty, K. Emery and Y. Yang, *Nat. Mater.*, 2005, **4**, 864.
84 Y. Kim, S. Cook, S. M. Tuladhar, S. A. Choulis, J. Nelson, J. R. Durrant, D. D. C. Bradley, M. Giles, I. McCulloch, C.-S. Ha and M. Ree, *Nat. Mater.*, 2006, **5**, 197.
85 J. Yang, R. Zhu, Z. Hong, Y. He, A. Kumar, Y. Li and Y. Yang, *Adv. Mater.*, 2011, **23**, 3465.
86 T. Liu and A. Troisi, *J. Phys. Chem. C*, 2011, **115**, 2406.
87 M. Böckmann, T. Schemme, D. H. de Jong, C. Denz, A. Heuer and N. L. Doltsinis, *Phys. Chem. Chem. Phys.*, 2015, **17**, 28616.
88 G. H. Wannier, *Phys. Rev.*, 1937, **52**, 191.
89 E. Blount, *Solid State Phys.*, Academic Press, 1962, vol. 13, p. 305.
90 N. Marzari and D. Vanderbilt, *Phys. Rev. B: Condens. Matter Mater. Phys.*, 1997, **56**, 12847.
91 P. L. Silvestrelli, *Phys. Rev. B: Condens. Matter Mater. Phys.*, 1999, **59**, 9703.
92 J. P. Perdew, K. Burke and M. Ernzerhof, *Phys. Rev. Lett.*, 1996, **77**, 3865–3868.
93 S. Grimme, *J. Comput. Chem.*, 2006, **27**, 1787.
94 N. Troullier and J. L. Martins, *Phys. Rev. B: Condens. Matter Mater. Phys.*, 1991, **43**, 1993.
95 I. Frank, J. Hutter, D. Marx and M. Parrinello, *J. Chem. Phys.*, 1998, **108**, 4060.
96 S. Grimm, C. Nonnenberg and I. Frank, *J. Chem. Phys.*, 2003, **119**, 11574.
97 C. Nonnenberg, S. Grimm and I. Frank, *J. Chem. Phys.*, 2003, **119**, 11585.
98 R. Car and M. Parrinello, *Phys. Rev. Lett.*, 1985, **55**, 2471.
99 S. Nosé, *J. Chem. Phys.*, 1984, **81**, 511–519.
100 W. G. Hoover, *Phys. Rev. B: Condens. Matter Mater. Phys.*, 1985, **31**, 1695.
101 W. Humphrey, A. Dalke and K. Schulten, *J. Mol. Graphics*, 1996, **14**, 33.
102 J. Stone, *MSc thesis*, Computer Science Department, University of Missouri-Rolla, 1998.
103 T. Kowalczyk, T. Tsuchimochi, P.-T. Chen, L. Top and T. Van Voorhis, *J. Chem. Phys.*, 2013, **138**, 164101.
104 M. Odelius, D. Laikov and J. Hutter, *THEOCHEM*, 2003, **630**, 163.
105 H. Langer and N. L. Doltsinis, *J. Chem. Phys.*, 2003, **118**, 5400.
106 N. L. Doltsinis, *Mol. Phys.*, 2004, **102**, 499.
107 I. Tavernelli, U. F. Röhrig and U. Rothlisberger, *Mol. Phys.*, 2005, **103**, 963.
108 P. R. L. Markwick, N. L. Doltsinis and J. Schlitter, *J. Chem. Phys.*, 2007, **126**, 045104.
109 H. Nieber and N. L. Doltsinis, *Chem. Phys.*, 2008, **347**, 405.
110 S. Rössle, J. Friedrichs and I. Frank, *ChemPhysChem*, 2010, **11**, 2011.
111 J. P. Perdew, M. Ernzerhof and K. Burke, *J. Chem. Phys.*, 1996, **105**, 9982.
112 C. Adamo and V. Barone, *J. Chem. Phys.*, 1999, **110**, 6158.
113 G. Torrie and J. Valleau, *J. Comput. Phys.*, 1977, **23**, 187.
114 J. Kästner and W. Thiel, *J. Chem. Phys.*, 2005, **123**, 144104.
115 J. Kästner, *Wiley Interdiscip. Rev.: Comput. Mol. Sci.*, 2011, **1**, 932.
116 D. Chandler, *J. Chem. Phys.*, 1978, **68**, 2959.
117 D. Frenkel and B. Smit, *Understanding Molecular Simulation*, Academic Press, San Diego, 2nd edn, 2002.
118 J. B. Watney, A. V. Soudackov, K. F. Wong and S. Hammes-Schiffer, *Chem. Phys. Lett.*, 2006, **418**, 268.
119 P. Hänggi, P. Talkner and M. Borkovec, *Rev. Mod. Phys.*, 1990, **62**, 251.
120 C. H. Bennett, *Molecular Dynamics and Transition State Theory: The Simulation of Infrequent Events*, American Chemical Society, 1977, ch. 4, p. 63.
121 M. Kac, *Am. Math. Mon.*, 1947, **54**, 369.
122 J. Liu, Y. Sun, X. Gao, R. Xing, L. Zheng, S. Wu, Y. Geng and Y. Han, *Langmuir*, 2011, **27**, 4212.
123 O. P. Dimitriev, *Nanoscale Res. Lett.*, 2017, **12**, 510.
124 L. Lüer, H.-J. Egelhaaf, D. Oelkrug, G. Cerullo, G. Lanzani, B.-H. Huisman and D. de Leeuw, *Org. Electron.*, 2004, **5**, 83.
125 P. E. Shaw, A. Ruseckas and I. D. W. Samuel, *Adv. Mater.*, 2008, **20**, 3516.
126 S. Cook, H. Liyuan, A. Furube and R. Katoh, *J. Phys. Chem. C*, 2010, **114**, 10962.
127 B. Baumeier, J. Kirkpatrick and D. Andrienko, *Phys. Chem. Chem. Phys.*, 2010, **12**, 11103.